Photoionization of monocrystalline CVD diamond irradiated with ultrashort intense laser pulse

Stefano Lagomarsino, Silvio Sciortino, Boyan Obreshkov, Tzveta Apostolova, Chiara Corsi, Marco Bellini, Eleni Berdermann, and Christian J. Schmidt

Phys. Rev. B **93**, 085128 — Published 22 February 2016

DOI: 10.1103/PhysRevB.93.085128

Photoionization of moncrystalline CVD diamond irradiated with ultrashort intense laser pulse

Stefano Lagomarsino and Silvio Sciortino
INFN and Department of Physics and Astronomy of Florence, Via Sansone 1, Sesto Fiorentino, Italy

Boyan Obreshkov
Institute for Nuclear Research and Nuclear Energy,
Bulgarian Academy of Sciences, Tsarigradsko chausseé 72, Sofia 1784, Bulgaria

Tzveta Apostolova
Institute for Nuclear Research and Nuclear Energy, Bulgarian Academy of Sciences,
Tsarigradsko chausseé 72, Sofia 1784, Bulgaria and
Institute for Advanced Physical Studies, New Bulgarian University, 21 Montevideo str., Sofia 1618, Bulgaria

Chiara Corsi
LENS and Department of Physics and Astronomy of Florence,
Via nello Carrara 1, 50019 Sesto Fiorentino, Italy

Marco Bellini
INO-CNR, Via nello Carrara 1, 50019 Sesto Fiorentino, Italy

Eleni Berdermann and Christian J. Schmidt
GSI, Darmstadt, Germany

Direct laser writing of conductive paths in synthetic diamond is of interest for implementation in radiation detection and clinical dosimetry.

Unraveling the microscopic processes involved in laser irradiation of diamond below and close to the graphitization threshold under the same conditions of the experimental procedure used to produce three-dimensional (3D) devices is necessary to tune the laser parameters to optimal results. To this purpose a Transient Currents Technique (TCT) has been used to measure laser-induced current signals in monocrystalline diamond detector in a wide range of laser intensities and at different bias voltages. The current transients vs. time and the overall charge collected have been compared with theoretical simulations of the carrier dynamics along the duration and after the conclusion of the 30 fs laser pulse. The generated charge has been derived from the collected charge by evaluation of the lifetime of the carriers. The plasma volume has also been evaluated by measuring the modified region.

The theoretical simulation has been implemented in the framework of empirical pseudopotential method extended to include time-dependent couplings of valence electrons to the radiation field. The simulation, in the low intensity regime, $I \sim 1$ TW/cm^2, predicts substantial deviation from the traditional multiphoton ionization, due to non-perturbative effects involving electrons from degenerate valence bands. For strong field with intensity of about 50 TW/cm^2, non-adiabatic effects of electron-hole pair excitation become prominent with high carrier densities eventually causing the optical breakdown of diamond.

The comparison of theoretical prediction with experimental data of laser generated charge vs. laser energy density yields a good quantitative agreement over six orders of magnitude. At the highest intensities the change of slope in the trend is explained taking into account the dependence of the optical parameters and the carrier mobility on plasma density.

PACS numbers: 72.20.Jv 29.40.Wk 32.80.Rm 42.50.Hz

I. INTRODUCTION

Three-dimensional (3D) diamond devices are fabricated by writing graphitic electrodes inside the diamond bulk by laser irradiation[1–3]. This is achieved in the femtosecond range, from 400 fs to 30 fs with apparently no damage of the surrounding diamond lattice that has been reported to occur in the nanosecond range[1,4]. The interest is mainly focused in producing radiation tolerant detectors in high energy physics and small field dosimeters for radiotherapy, although other applications as IR photonic crystals[5,6] and microsystem devices[7] have also been proposed. 3D diamond detectors combine the intrinsic properties of radiation tolerance of diamond with the advantages of the 3D architecture. In 3D detectors a shorter interelectrode distance results in a lower voltage bias required to collect the charge produced in the diamond thickness. Because of the reduced path of the charge

carriers, the charge loss is minimized and the Charge Collection Efficiency (CCE) increased, as a consequence, 3D diamond detectors can be can be the radiation hardest sensors ever implemented[8]. Moreover, due to the high saturation velocity of carriers in diamond[9], they are particularly interesting in subnanosecond timing applications. The resistivity of the electrodes, that is of the order of 1 -0.1 Ωcm[4,10], i.e. orders of magnitude higher than the typical resistivity of microcrystalline graphite, can represent a major drawback for these applications, resulting in electric noise of the tracker detector and limiting the resolution in time-of-flight measurements.

The subject is intensely studied at present, but despite of many experimental efforts a clear understanding of the relationship between properties of the modified material and laser parameters is lacking. Only one theoretical model on diamond graphitization has been proposed so far, involving single photon excitation above bandgap[11,12], which is an experimental condition distant from the cited experimental conditions and applications, because irradiation below bandgap is needed to produce electrodes inside the diamond bulk. The material modified by irradiation that we loosely refer to as graphitic is also ill-defined, apart from the notion that is a mixed phase of sp^2 and sp^3 bonds[4]. Experimental evidence points out that it is possible to set some figures-of-merit as resistivity of the bulk electrodes, CCE of the obtained sensors, that are likely related to the presence or absence of local damage of the diamond lattice around the graphitic material. This in turn can be related to and depend more or less critically on the various laser parameters: energy per pulse, pulse width, repetition rate, speed of advance of the laser waist, presence of optical aberration. The original material properties of the diamond lattice are also very critical, since the energy threshold for graphitization, the volume of the modified material and its resistivity depend on the polycrystalline or monocrystalline nature of the sample. The energy threshold varies if the graphitization is started from the surface or in the bulk and also vary within the samples of the same batch, in the polycrystalline case, or even in the same sample at different points, suggesting a strong dependence on defects which can lower sensibly the energy required to initiate the phase transition.

A deep understanding of the physics of the processes is required to tune the laser parameters, in order to obtain the sought properties of the electrodes inside the diamond bulk and achieve a reliable and reproducible procedure to implement optimal devices. These are the processes of excitation and recombination of carriers, release of energy to the lattice and modification of the chemical bond. It is also critical to take into account the different crystalline qualities of the diamond samples available, which can be determined by their original optical and electronic properties.

As a first step towards achieving this understanding we have carried out a combined theoretical and experimental study on the laser excitation of carriers over a three orders of magnitude interval of energy per pulse, resulting into a six orders of magnitude variation in induced charge. Carriers generated in monocrystalline diamond by single laser pulses have been collected with a Transient Current Technique (TCT). The generated charge has been calculated from the measured one, after evaluation of the carrier's lifetime. The higher energies per pulse used are quite above the graphitization level of diamond on the free surface and of the graphitization threshold for the polycrystalline bulk, but below the graphitization level of pure monocrystalline diamond bulk. In this way we demonstrate that the 3D diamond devices fabricated so far depend on the presence of defect seeds. The experimental results are simulated with a quantum theoretical model of multi-photon excitation across the diamond bandgap. At the highest energies it is also necessary to take into account the change in optical parameters of the diamond caused by the high concentration of carriers. In fact, similar to what is observed in other materials[13], non-linear absorption causes a relevant amount of energy to be deposited prior to the focus. As a consequence, we do not reach the energy density required to the phase transition in the pure diamond bulk. The quantum theoretical model, together with the high energy correction, is in agreement with the experimental data over a very wide energy and corresponnding carrier density range, resulting in the first quantitative validation of a theoretical model of multi-photon excitation of diamond to our knowledge. This result opens the way to a full understanding of laser graphitization by femtosecond pulses, a subject relevant also beyond the suggested applications. Diamond is a cardinal material with ever growing experimental applications and the process of laser graphitization is generally important, even when it is an unwanted side effect.

The paper is organized as follows: in Sec. II, we present our experimental setup, Sec. III discusses transient current measurements, Sec. IV presents numerical results for the photoionization yield in the irradiated diamond and Sec. V discusses the validation of the theoretical model by means of the experimental data.

II. EXPERIMENTAL SETUP

The experimental setup used is a modification of a reported TCT system[14] . A monocrystalline diamond detector is biased at different voltage values, from 0 to 550 V, corresponding to a mean electric field ranging from 0 to 1.1 V/μm, i.e., up to values at which the carriers are close to their saturation velocities. We used electronic grade monocrystalline diamond material, from Element Six UK ($4.5\times4.5\times0.5$ mm^3). These samples exhibit a typical dark current of the order of picoamperes at the maximum voltage. Charge carriers were produced by laser irradiation, after focusing a laser beam inside the diamond bulk. The current vs. time was acquired by a broadband (1 GHz) oscilloscope. At low laser fields

a 2.5 GHz, 40 dB amplifier was used. In this way it was possible to span four orders of magnitude of current intensity. The lower current signal detectable due to electronics noise was about 2 μA and the highest measured 23 mA. A Ti-sapphire mode-locked laser source with central wavelength of 800 nm and a pulse width of 30 fs at the laser output has been used for excitation. The energy densities at a beam waist diameter of about 5 μm were in the range of 0.08-51 J/cm^2, the corresponding energy per pulse at the focus inside the samples ranged from 8 nJ to 5 μJ. Two electronic grade CVD diamond samples were used for the measurements of the transient currents induced by laser irradiation. The first diamond plate was irradiated through the 4.5 $\times$4.5 mm^2 major faces and the voltage bias was applied between graphitic electrodes previously fabricated by laser in the diamond bulk. This arrangement suffered of an uncertainty due to non-homogeneous electrostatic field. Moreover, since the sample is only 0.5 mm thick, its surface was too close to the focus and, with increasing the laser field intensity was often unintentionally damaged. In fact, due to surface defects the graphitization threshold of the surface is in the range 2-4 μJ/pulse, i.e. quite lower than that of the diamond bulk as we will discuss below. To avoid these drawbacks we used a second diamond plate, with 4$\times$ 4 mm^2 metal contacts fabricated on the opposite major faces and the fs laser was focused inside the bulk, between the electrodes, through an optically polished 0.5 $\times$4.5 mm^2 lateral face. In this way it was possible, to focus the laser in a region of uniform electrostatic field and sufficiently far from the face to avoid its damage. The new measurements turned out to be fully consistent with the ones carried out with the previous sample. We found that the main variation of the experimental points is due to the unpredictable variation of the laser wavefront from an ideal gaussian profile due to the fact that measurements on a same sample were performed in different periods after a time interval of several months and it was not possible to exactly reproduce the same condition of the laser source. This effect scatters the data points taken with the same sample more than the spread between data corresponding to different samples. The experimental data points are shown in Fig. 4 and will be further discussed. The current and the charge collected at the electrodes was measured at different field intensities and bias voltages. The intensity in the sample was varied by interposing calibrated filters in the optical path and by changing the laser pump intensity. The stability of the laser output was monitored by means of a silicon photodiode which was also used to trigger the acquisition of the current and charge waveforms.

III. TRANSIENT CURRENT MEASUREMENTS

Typical current transients $i(t)$ at low intensities are shown in Fig. 1 at a voltage bias of $V = V_{\max} = 550$ V. Curves taken at lower intensities could be visible only in a logarithmic scale. The waveforms maintain the same shape at different laser intensities.

The rising part of the current waveform can be fitted to a $\sqrt{t}$ trend and the decaying part to a curve $\sqrt{T-t}$ (with different proportionality constants), where T is the time interval over which the current is non-vanishing. This behavior can be explained with a competition between diffusion of the generated carriers and drift along the electrostatic field which is due to the external bias and the space charge itself.

In Fig. 2, we have superimposed the current waveforms at higher laser intensities. Their lineshape is different from the low intensity waveform, nonetheless it remains quite the same at higher bias voltages (lower transit times), provided that a scale factor is taken into account. Fig. 3 shows the variation of the current waveform at different voltage bias from 100 V to 550 V at an energy per pulse E=8 nJ. It is evident that the curves at 400 V and 550 V have the same shape, while at lower voltages they exhibit a more pronounced decaying tail.

The time window T of the transient current decreases with increasing bias voltage and velocity of the carriers. Conversely, T increases with the laser intensity. This is due to the high density of the plasma generated by the field and the increasing mutual attraction between holes and electrons. For higher laser fields, as the electron-hole density becomes larger, some recombination/trapping occurs, because the transit time T becomes comparable with the lifetime τ of the generated electron-hole plasma, at any applied voltage. The generated charge $Q(0)$ during the laser pulse, at $t \approx 0$, can be derived from the collected charge $Q = \int_0^T i(t')dt'$ as shown in the appendix. We define Q as the collected charge at a given voltage bias V, which is a constant, not to be confused with the transient electronic charge $Q(t)$.

In Fig. 4 we plot the collected charge Q (open circles) vs. the energy per pulse E, at a bias voltage of 500 V, in a Log-Log scale. The calculated charge $Q(0)$ (filled squares) has also been reported. The correction is appreciable for higher energy-per-pulse values, as T becomes comparable to the average time τ of recombination/trapping, up to a factor of 60%. However, after this correction, we still observe a definite change of slope around $E = 0.1$ μJ/pulse, which is actually reflecting the physics of the excitation process.

In order to connect the experimentally generated charge $Q(0)$ to the carrier density we need a correct determination of the volume of the plasma region involved in the excitation. We assume that the laser wavefront can be represented to a good approximation by a gaussian function. In order to evaluate the beam waist radius w_0 and the Rayleigh range is z_R we irradiated the bulk of a polycrystalline diamond plate in different positions through a lateral polished face and observed the irradiated regions through the bases. In the polycrystalline material, the graphitization threshold of the bulk is lower than in the monocrystalline diamond, and strongly varies

from point to point within the same sample, due to the high concentration of defects in the polycrystalline structure. This allowed us to graphitize different regions of the sample within an energy range from 1.6 to 8.5 μJ/pulse. The lower threshold corresponded to a minimal graphitized volume which can be reasonably taken as a good estimate of the plasma volume. An optical micrograph of the laser modified region is shown in Fig. 5. The ellipsoidal-shaped volume is consistent with a value of the depth of focus $z_R = 35\mu$m and a value of the waist radius $w_0 \approx 2.5$ μm.

IV. THEORETICAL MODEL

For the relatively short duration of the laser pulse (30fs) considered in this work we assume that the nuclei remain fixed at the lattice points during the irradiation, such that energy is absorbed from the laser field via creation of electron-hole pairs. We also neglect the contribution of impact ionization to the population of the conduction band. It has been predicted that avalanche generation in dielectrics is less important than strong-field ionization for pulse durations below 100 fs[15,16]. However, there is experimental evidence that optical breakdown in fused silica is dominated by avalanche ionization down to the 10 fs regime[17]. In particular the observed multiphoton ionization rates were found substantially lower than those predicted by Keldysh theory, thus identifying non-perturbative mechanism of carrier generation in bulk silica. Moreover, in a recent work on non linear absorption of femtosecond laser pulses in silica[18] transmission curves at different pulse durations have been fitted to a model taking into account multiphoton absorption and impact ionization through a modified rate equation. The results were consistent with a photon-assisted avalanche ionization rate that increases with decreasing pulse length down to a 10 fs time scale. Nevertheless, we will show, in Sec. V A , that the physical conditions under which the prominence of impact ionization occurs in silica are very different from those encountered in diamond, at the same laser intensities. In fact, even if the kinetic energy distribution of the photoexcited carriers extends above the required threshold, the process of impact ionization is strongly suppressed by the high population of the conduction band low energy states, due to Pauli blocking. In Sec. V B, we will present evidence that the approximation of neglecting impact ionization is able to provide good quantitative agreement with the measured photoionization yield in diamond.

Recently[19], it was experimentally found that high-harmonic generation in bulk solids is characteristic of a non-perturbative quantum interference process that involves electrons from multiple valence bands. Thus in order to clearly distinguish field-assisted collisional effects from coherent process in the laser-irradiated diamond, we investigate the quantum dynamics of the microscopic polarization and charge carrier distribution in one-particle framework by incorporating realistic substrate band-structure.

In long wavelength approximation we represent the light pulse by a spatially uniform time-dependent electric field. The coupling of electrons to the laser field is modelled in single-particle approximation based on the Hamiltonian

$$H(t) = \frac{1}{2}(\mathbf{p} + \mathbf{A}(t))^2 + V(\mathbf{r}) \tag{1}$$

including the periodic ion-lattice potential

$$V(\mathbf{r}) = \sum_{\mathbf{G}} V(G)\cos(\mathbf{G}\cdot\boldsymbol{\tau})e^{i\mathbf{G}\cdot\mathbf{r}}, \tag{2}$$

where $2\boldsymbol{\tau} = a_0(1/4, 1/4, 1/4)$ is a relative vector connecting two carbon atoms in a crystal unit cell, $a_0 = 3.57\mathring{A}$ is the bulk lattice constant for diamond and $\mathbf{G}$ labels the reciprocal lattice wave-vectors. We apply the empirical pseudopotential method to describe the atomic form factors $V(G)$[20,21]. Velocity gauge implied by Eq.(1) is used throughout our calculation[22] and the time-dependent electronic wave-function is expanded over Bloch states of definite crystal momentum $\mathbf{k}$

$$\psi(\mathbf{r}, t) = \sum_{n\mathbf{k}} a_{n\mathbf{k}}(t)e^{i\mathbf{k}\cdot\mathbf{r}}u_{n\mathbf{k}}(\mathbf{r}), \tag{3}$$

where $u_{n\mathbf{k}}$ is the lattice-periodic part of the Bloch wavefunction

$$u_{n\mathbf{k}}(\mathbf{r}) = \sum_{\mathbf{G}} e^{i\mathbf{G}\cdot\mathbf{r}}c_{n,\mathbf{G}+\mathbf{k}}, \tag{4}$$

expressed in terms of Fourier coefficients satisfying

$$\frac{1}{2}(\mathbf{G}+\mathbf{k})^2 c_{n,\mathbf{G}+\mathbf{k}} + \sum_{\mathbf{G}'} V_{\mathbf{G}-\mathbf{G}'}c_{n,\mathbf{G}'+\mathbf{k}} = \varepsilon_{n\mathbf{k}}c_{n,\mathbf{G}+\mathbf{k}}, \tag{5}$$

with eigen-energies $\varepsilon_{n\mathbf{k}}$ specifying the static substrate band structure. The time-evolution of the Fourier amplitudes

$$i\partial_t a^{(m\mathbf{k})}_{n\mathbf{k}}(t) = \varepsilon_{n\mathbf{k}}a^{(m\mathbf{k})}_{n\mathbf{k}}(t) + \sum_{n'} \mathbf{A}(t)\cdot\mathbf{p}_{nn'}(\mathbf{k})a^{(m\mathbf{k})}_{n'\mathbf{k}}(t), \tag{6}$$

is subject to initial conditions specified long before the start of the pulse $a^{(m\mathbf{k})}_{n\mathbf{k}}(t \to -\infty) = \delta_{nm}$ and the matrix representation of the momentum operator is

$$\mathbf{p}_{nn'}(\mathbf{k}) = \mathbf{k}\delta_{nn'} - i\frac{1}{\Omega_{u.c.}}\int_{\Omega_{u.c.}} d^3\mathbf{r}\, u^*_{n\mathbf{k}}(\mathbf{r})\nabla_{\mathbf{r}}u_{n'\mathbf{k}}(\mathbf{r}), \tag{7}$$

with off-diagonal matrix elements describing interband transitions, $\Omega_{u.c.} = a_0^3/4$ is the volume of the unit cell. The occupation numbers of single-particle states at time t are

$$f_{n\mathbf{k}}(t) = \sum_{m=1}^{M} |a^{(m\mathbf{k})}_{n\mathbf{k}}(t)|^2, \tag{8}$$

where M is the total number of in initially occupied valence bands. The total number of electrons that have been photo-excited into the conduction band is given by the Brillouin zone (BZ) integral

$$n_e(t) = \sum_{n=M+1}^{\infty} \int_{\rm BZ} \frac{d^3\mathbf{k}}{(2\pi)^3} f_{n\mathbf{k}}(t). \quad (9)$$

Charge neutrality implies that the total number of valence band holes is equal the total number of conduction electrons, i.e. $n_h = n_e$.

V. NUMERICAL RESULT AND DISCUSSION

A. Outcome of the model

We evaluate the substrate band structure in a plane-wave basis with kinetic-energy cut-off 35 Ry. The pseudopotential form factors $V(G)$ used for diamond (in Rydbergs) are $V(G^2 = 3) = -0.625$, $V(G^2 = 8) = 0.051$ and $V(G^2 = 11) = 0.206$, here the wave-number G is given in units of $2\pi/a_0$. The time-dependent electron density is represented in a basis of static Bloch orbitals including 4 valence and 16 conduction bands, and the time-integration of the Schrödinger equation is performed by applying the Crank-Nicolson method for small equidistant time steps $\delta t \approx 1$ attosecond. The BZ integration is carried out by a simple Monte Carlo method using 1500 randomly generated $\mathbf{k}$-points in a cube of edge length $(4\pi/a_0)$. The time-profile of the laser field is modelled by a Gaussian function

$$\mathbf{A}(t) = \mathbf{e}A_0 \sin(\omega_L t) e^{-\ln(4)t^2/\tau_L^2}, \quad (10)$$

where $\mathbf{e}$ is a unit vector pointing in the direction of the electric field, the photon energy related to the driving frequency is $\hbar\omega_L = 1.55$ eV, the pulse duration is $\tau_L = 30$ fs and the field strength A_0 is given by the peak intensity of the laser field with $I = c\omega_L^2 A_0^2/(8\pi)$ where c is the speed of light in vacuum.

In Fig.6, we show the static band structure for crystal momentum $\mathbf{k}$ changing along the ΓX and ΓL directions in the bulk BZ. The empirical pseudopotential model reproduces quantitatively the principal energy gaps of this band structure. The location of the conduction band minimum at $\mathbf{k} \approx (0.8, 0, 0)2\pi/a_0$ corresponds to an indirect gap of 5.42 eV, that is in very good quantitative agreement with the experimental result ($E_{\rm gap} = 5.45$ eV). Since in long-wavelength approximation the laser cannot induce a momentum changing transition, the minimal energy required to surpass the energy gap at the Γ point is 7 eV. For relatively low intensity of the laser field $I \ll 100$ TW/cm^2, excitation of valence electrons across this gap should occur via 5 photon absorption according to the Keldysh theory[23].

In Fig.7 we plot the time evolution of the electron density $n_e(t)$ for linearly polarized laser field, directed parallel to the bonds between carbon atoms, and for three different intensities $I = 1.5$ TW/cm^2, $I = 10$ TW/cm^2 and $I = 50$ TW/cm^2. The total number of electrons excited to the conduction band increases on the rising part of the pulse. At a later time, the charge density oscillations follow the time periodicity of the incident radiation. These transient charge oscillations are exclusively due to the time-dependent shift of the momenta of valence electrons $\mathbf{k} \to \mathbf{k} + \mathbf{A}(t)$, which adjust instantaneously (adiabatically) to the slow variation of the vector potential. Due to this velocity boost, the overlap among shifted valence and undistorted conduction bands $\langle c\mathbf{k}|v\mathbf{k}(t)\rangle$ oscillates with the periodicity of the laser field. During one half-cycle of the pulse, some fraction of electrons is transferred back into the valence band and deviation from the adiabatic time-evolution occurs at the extrema of the electric field. The photo-ionization yield stabilizes in the wake of the pulse. Photoionization is less likely for lower field intensities ($I < 10$ TW/cm^2), since valence electrons do not gain sufficient energy from the field to be excited into the conduction band. That is because of the wide bandgaps of diamond, which favor adiabatic time evolution resulting in relatively small final electron yields $n_e \sim 10^{18}$ cm^{-3}. Non-adiabatic effects of electron-hole pair creation depend very sensitively on the laser intensity. When the intensity is raised above $I \geq 50$ TW/cm^2 the occupation of the conduction band becomes prominent resulting in high photoionization yields with $n_e \sim 10^{21} cm^{-3}$ after the conclusion of the pulse.

In Fig.8 we plot the time-dependent macroscopic polarization density $P(t) = \int_{-\infty}^{t} dt' J(t')$, which gives the charge transferred into the conduction band per unit area at time t. The macroscopic current density $J(t)$ in the direction of the electric field is given by an average over the volume of the unit cell

$$J(t) = \frac{1}{\Omega_{u.c.}} \int_{\Omega_{u.c.}} d^3\mathbf{r}\ \mathbf{j}(\mathbf{r}, t) \cdot \mathbf{e}, \quad (11)$$

where the space- and time-dependent electron current density

$$\mathbf{j}(\mathbf{r}, t) = \sum_{m\mathbf{k}} \frac{1}{2} \left[\psi^*_{m\mathbf{k}}(\mathbf{r}, t)(-i\nabla_{\mathbf{r}} + \mathbf{A}(t))\psi_{m\mathbf{k}}(\mathbf{r}, t) + c.c\right], \quad (12)$$

is given by the sum over initially occupied valence band orbitals. For relatively low intensity of the laser pulse $I \approx 2$ TW/cm^2, the polarization follows adiabatically the applied electric field. For the increased pulse intensity $I = 10$ TW/cm^2, the dielectric response of the crystal remains predominantly linear with no noticeable sustained current of delocalized electrons after the end of the pulse. When the intensity is increased to $I = 50$ TW/cm^2, the polarization density exhibits almost linear time dependence in the wake of the pulse, showing that a DC current is generated. Similar results are found in TDDFT simulations predicting generation of ultrafast currents in silica after the irradiation with few-cycle laser pulses[24]. The induced DC current will eventually heat up the diamond lattice due to electron-phonon interactions[25] on

a longer time scale, which we neglected in the present simulation.

The momentum distribution of photoionized electrons in the wake of the pulse is shown in Fig.9 for two specific directions in the bulk BZ for linearly polarized laser field parallel to C-C bonds. For the lowest shown intensity $I \sim 1$ TW/cm^2 in Fig.9(a), the conduction band remains nearly empty with no significant electronic excitation, electrons are ionized with momenta close to the BZ centre. For the increased intensity $I = 10$ TW/cm^2, shown in Fig.9(b), the occupation of the conduction band becomes substantial and electrons redistribute over momenta to favor states away from the BZ centre. If the intensity is increased to 50 TW/cm^2, cf. Fig.9(c), the distribution broadens in momentum space and moves toward the BZ edges. This leads to the conclusion that significant contribution to the total electron yield is due to transitions not occurring in the centre of BZ, consistently with the semi-analytic results in Ref.[26].

The density of conduction band states at the end of the pulse is shown in Fig.10(a-c) for parallel polarization of the laser. For $I \sim 1$ TW/cm^2 shown in Fig.10(a), the distribution displays an isolated Lorentzian peak located at 1.5 eV above the conduction band minimum, reflecting the fact that in this regime transitions occur near the BZ centre. For the increased field intensity in Fig.10(b) $I = 10$ TW/cm^2, the position of the low-energy peak is unaffected, however the Lorentzian profile is distorted by the laser pulse and is supplemented by additional satellite structures on the low and high energy sides of the central peak. For the higher pulse intensity $I = 50$ TW/cm^2 shown in Fig.10(c), the density of conduction band states extends due to release of electrons with higher kinetic energies. Since the excess kinetic energy of the photoexcited carriers is above threshold for impact ionization, the subsequent energy loss during binary encounters would limit this energy distribution within the bulk. However, since large fraction of electrons have already been photoexcited close to the conduction band minimum, the scattering probabiltiy into these low-energy states is reduced due to Pauli blocking. Thus for high level of electronic excitation the probability for impact ionization should become unlikely, such that electrons can gain sufficiently high energies from the laser field.

In Fig.11 we show the photoionization yield as a function of the pulse intensity I for parallel polarization of the electric field. In the low intensity regime $I < 1$ TW/cm^2, the electron yield increases linearly with the increase of I due to highly suppressed one-photon ionization (with negligible final densities $n_e \leq 10^{14} cm^{-3}$). The photoionization probability raises steeply with the increase of the intensity in the range $I = 1$ TW/cm^2 - $I = 2$ TW/cm^2.

The slope of the theoretical curve can be fitted to $n \sim I^N$ scaling law over that range, with $N = 9$ corresponding to 9-photon ionization, showing that a deviation from the perturbative scaling law I^5 occurs, pointing out that electron promotion across the diamond bandgaps is sensitive to the detailed characteristics of the substrate band-structure (cf. also[27,28]). For $I \approx 3$ TW/cm^2 ionization becomes unlikely, as the electron yield decreases by one-order of magnitude. That is because interband transitions occur away from the Γ point, where the wide bandgaps of diamond (~ 10 eV) suppress ionization. For increased light pulse intensities $I > 5$ TW/cm^2, the slope of the curve flattens out as function of I. In this high-intensity regime, the momentum distribution of ionized electrons becomes more diffuse and extends over the entire Brillouin zone. When $I = 50$ TW/cm^2 the carrier densities are $n_e \geq 10^{20} cm^{-3}$, showing that dielectric breakdown occurs[29]. Indeed for such high conduction electron density, the corresponding bulk plasma frequency $\omega_p = (4\pi n_e)^{1/2}$ matches the laser frequency ω_L, such that electrons can absorb very efficiently energy from the light pulse via excitation of bulk plasmon resonance.

To provide further insight on the mechanisms leading to the non-perturbative I^9 scaling law in the low-intensity regime $I \sim 1$ TW/cm^2, we consider a simplified two-band model taking into account the three-fold degeneracy of the valence band at the Γ point, i.e.

$$i\partial_t a_{v_i} = \mathbf{A}(t) \cdot \mathbf{p}_{v_i c} a_c(t)$$
$$i\partial_t a_c = \Delta a_c + \sum_{i=1}^{3} \mathbf{A}(t) \cdot \mathbf{p}_{c v_i} a_{v_i}(t)$$

and $\Delta = 7$ eV is the bandgap. Direct interactions among valence bands vanish because of the even symmetry of their wave-functions under spatial inversion. The equation of motion for the photoionization amplitude can be integrated formally with the result

$$a_c(t) = -i \sum_{i=1}^{3} \int_{-\infty}^{t} dt' e^{-i\Delta(t-t')} \mathbf{A}(t') \cdot \mathbf{p}_{c v_i} a_{v_i}(t') \quad (13)$$

such that the time-evolution of the valence band amplitudes becomes

$$\partial_t a_{v_i} = -\mathbf{A}(t) \cdot \mathbf{p}_{v_i c} \sum_{j=1}^{3} \int_{-\infty}^{t} dt' e^{-i\Delta(t-t')} \mathbf{p}_{c v_j} \cdot \mathbf{A}(t') a_{v_j}(t'), \quad (14)$$

showing that the Stark mixing has introduced indirect dipole-dipole couplings among valence bands for $v_i \neq v_j$. In Fig. 12(a) we plot the time-evolution of the absolute value of the Fourier amplitudes (for laser intensity $I = 1.5$ TW/cm^2) by neglecting the effect of induced dipole couplings. For this low intensity of the laser field, the valence band is only weakly distorted hence photoexcitation into the conduction band is highly unlikely. In contrast, the strong indirect interaction among Stark-mixed valence bands enables the photoionization of bulk diamond as shown in Fig. 12(b).

The enhancement of the photoionization yield is also exhibited in the time-evolution of the optically induced interband polarization in the wake of the pulse in

Fig. 12(c). Due to the induced dipole-dipole interactions between valence bands, the polarization displays rapid time oscillations with period corresponding to the bandgap energy 7 eV, otherwise it follows adiabatically the laser electric field. Thus by neglecting the induced dipole couplings, the Fourier transform of the interband polarization in Fig. 12(d) exhibits characteristic perturbative behavior, it includes 1st,3rd and 5th harmonics with rapidly decreasing intensities. This is in accord with the conventional Keldysh theory, which neglects energy-level degeneracies in the substrate band structure. Noticeably however, laser-induced interactions among valence bands produces non-perturbative harmonics in the Fourier transform of the induced polarization, with enhanced 5th harmonic relative to the 3rd one. This effect is substantial, since the 5th harmonic is enhanced by nearly 2 orders of magnitude relative to the conventional perturbative multiphoton result. Thus, dipole couplings between degenerate valence bands create a highly polarizable intermediate state, that ionizes very efficiently, under the light pulse, to produce the free electrons in the conduction band. It is worth to note that similar results are found in Ref.[30], showing that a strong, few-cycle optical field is capable of transforming silica into a state of highly increased polarizability.

B. Comparison with experiment

We now compare the theoretical calculations of the ionization yields n_e reported in Fig. 11 as a function of intensity I and the measured generated charge Q reported in Fig. 4 as a function of the energy per pulse E. For this purpose, we consider the space-dependence of the laser intensity in proximity of the beam waist. Since the charge diffusion length during the pulse is much smaller than both of the waist diameter and of the wavepacket length, we can consider the generated charge density as only dependent on the local energy density, defined as $\phi(r,z) = I(r,z)\tau_L$, with r the distance from the beam axis and z the position along the beam. Thus, we can write:

$$Q = \int_{-\infty}^{\infty} dz \int_0^{\infty} 2\pi r dr \cdot n_e\left(\phi(r,z)\right) \tag{15}$$

In Eq. 15, we considered a gaussian beam profile attenuated by a factor exponentially decreasing with the absorption length:

$$\phi(r,z) = \frac{2E}{\pi w_0^2\left(1+\frac{z^2}{z_R^2}\right)} \exp\left[-\frac{2r^2}{w_0^2\left(1+\frac{z^2}{z_R^2}\right)}\right] \times \\ \times \exp\left[-\frac{4\pi}{\lambda_0}\int_{-\infty}^{z} \kappa(r',z')dz'\right] \tag{16}$$

where λ_0 is the wavelength in vacuum. The constants w_0 and z_R have been evaluated measuring the size of the graphitized region of a polycrystalline diamond at the bulk graphitization threshold (Fig 5), which are respectively about 2-3 and 35 μm as anticipated in Sec. III. The extinction coefficient κ has been assumed to depend on the plasma density n_e, along with the refractive index n, according to the formulas:

$$\begin{aligned} n^2+\kappa^2 &= n_0^2 - \left(\omega_p/\omega_L\right)^2 \\ 2n\kappa &= \omega_p^2/\omega_L^3 \tfrac{e}{\mu m^*} g, \end{aligned} \tag{17}$$

where $\omega_{p,L}$ are respectively the plasma and the laser frequencies, μ and m^* are the mobility and the effective mass of the charge carriers, respectively, and $g \sim 1$ is a constant, depending on the scattering mechanism[31]. In Eq. 17 the mobility μ is a relevant term, decreasing by two orders of magnitude[32] when n_e increases from 10^{16} to 10^{19} cm^{-3}. As a consequence, when the generated charge density reaches the order of 10^{19} cm^{-3}, the absorption length becomes smaller (possibly much smaller) than z_R, and the laser pulse is absorbed long before reaching the region of the lase waist. At these densities, the plasma frequency is as low as between 1/7 to 1/3 of ω_L, and the refractive index differs negligibly from its static value 2.42. This justifies the assumption of negligible reflection-diffraction effects implied by Eq. 16. Note that n depends on ϕ in Eq. 15, and ϕ depends on the density n via the extinction coefficient in Eq. 16. Self-consistency is ensured if, along each ray path, we calculate values of $\phi(r,z)$ for increasing values of z, taking into account the previously calculated values of $\kappa(r',z')$ (and thus n, and ϕ) for $z' < z$.

Fig. 13 shows the final comparison of theory with experimental data. The three curves reported correspond to the charge calculated from Eq. 15 with w_0=2, 2.5 and 3 μm, z_R=35 μm. The $Q(0)$ values derived from the experiment, previously shown in Fig. 4, are also shown together with the theoretical charge values calculated assuming a carrier density equal to the ionization yield n in Fig. 11, uniformly distributed in an ellipsoidal volume element of axis $w_0 = 2.5\,\mu$m and $z_R = 35\,\mu$m.

The following considerations hold.

When the energy of the pulse is below 0.2μJ, the calculated behavior follows quite closely the values evaluated from n with the effective area, $A = \pi w_0^2/2$ and volume $4/3Az_R$ of the waist region. Nevertheless, considering the integrated Q given by Eq. 15, some features in the electron distribution such as the sharp dip are smeared out.

Above 0.2 μJ, when the laser pulse is absorbed before reaching the waist region, most of the pulse energy is spent to heat the already generated free-carriers, such that the overall charge increases much slower than suggested by the effective volume and area model. In fact, it grows as the first power of E, instead of $E^{2.4}$.

For reasonable values of the beam parameters, the calculated charge is close to the measured one over three orders of magnitude in pulse energy and six orders of magnitude in generated charge. The most critical region is the one with the higher slope because for these values

of the pulse energy the generated charge is expected to be strongly dependent on the beam optics.

VI. CONCLUSION

We investigated experimentally and theoretically the photo-ionization of monocrystalline CVD diamond subject to intense femtosecond laser irradiation. The experimental measurements were carried out under the very same conditions used for preparing three-dimensional devices by fabricating conductive columnar electrodes via laser bulk graphitization. The theoretical model can explain the experimental data starting from low pulse energies and reaching about E= 0.2 μJ,with a focus area of about 10 μm^2. For higher intensities, up to E=5 μJ, the theory correctly explains the experiment when pulse absorption due to the high plasma density is phenomenologically taken into account. The agreement of the data with the theory extends over six orders of magnitude in terms of generated charge and three orders of magnitude in terms of laser intensity. The graphitization threshold is not reached in the bulk because non-linear absorption limits the intensity of the laser field and energy is deposited before reaching (i.e. upstream of) the focus. On the contrary, when we prepare the devices the laser is initially not focused inside the diamond bulk but the conductive column is started from a localized region in the diamond surface where surface defects act as seeds. In order to fully explain the graphitization process it is mandatory to include a model for the defects involved. Our theoretical approach neglects electron-electron collisions on a femtosecond timescale which eventually cause the electron avalanching in diamond. Although all these complex mechanisms are not fully included in the simulations, we find that the experimental data is quantitatively described within our model incorporating realistic bulk band structure of diamond. Moreover we find that the Stark effect creates a highly polarizable transient state of bulk diamond that ionizes very efficiently under the light pulse. A complete understanding of the physics involved is required to tune the experimental parameters for preparing devices that can be used for particle detection and dosimetry.

Appendix: Determination of the initial charge $Q(0)$

Here we present formal derivation of the generated charge $Q(0)$ at the end of the laser pulse at $t = 0$, from the measured charge $Q = \int_0^T i(t')dt'$. Let $Q(t)$ be the plasma charge after a time interval t from the laser pulse and τ the electron-hole recombination/trapping time according to:

$$\dot{Q}(t) = -i(t) - \frac{Q(t)}{\tau}, \tag{A.1}$$

The dependence of the charge and current on the bias voltage V is left implicit in Eq. A.1. The solution is

$$Q(t) = e^{-\frac{t}{\tau}} \left(Q(0) - \int_0^t i(t') e^{\frac{t'}{\tau}} dt' \right). \tag{A.2}$$

Since $Q(T) = 0$, from Eq. A.2 we have

$$Q(0) = \int_0^T i(t') e^{\frac{t'}{\tau}} dt'. \tag{A.3}$$

We did not acquire $i(V, t)$ at all voltages, but since the lineshape is preserved in changing the voltage bias we can derive the current at a given bias, from the current at 550 V assuming the scale transformation:

$$i(t) = \frac{Q}{Q_M} \frac{T_M}{T} i_M \left(T_M \frac{t}{T} \right) \tag{A.4}$$

where $T_M, i_M(t), Q_M$ denote the quantities $T, i(t), Q$ corresponding to $V = V_{\max}$. The factor Q/Q_M is introduced to take into account the fact that the integral of the current is not independent of the voltage due to recombination. Since the generated charge does not depend on V we can write:

$$Q(0) = \int_0^T i(t') e^{\frac{t'}{\tau}} dt' = \int_0^{T_M} i_M(t') e^{\frac{t'}{\tau}} dt' \tag{A.5}$$

We can substitute expression A.4 into Eq. A.5:

$$\frac{T_M}{T} \frac{Q}{Q_M} \int_0^T i_M \left(T_M \frac{t'}{T} \right) e^{\frac{t'}{\tau}} dt' = \int_0^{T_M} i_M(t') e^{\frac{t'}{\tau}} dt' \tag{A.6}$$

From Eq A.6, performing integration by substitution, we obtain Q as a function of T:

$$Q = Q_M \frac{\int_0^{T_M} i_M(t') e^{\frac{t'}{\tau}} dt'}{\int_0^{T_M} i_M(t') e^{\frac{t'}{\tau}} \frac{T}{T_M} dt'} \tag{A.7}$$

Eq. A.7 is reasonably valid for $T \approx T_M$, i.e., for low transit times. At higher T we observe current lineshapes slightly distorted, so that the scaling assumption A.4 fails to be satisfied. Hence, we can use a linear approximation of the expression of the collected charge:

$$Q = Q_M - (T - T_M)a \tag{A.8}$$

where the slope a:

$$a = \frac{Q_M}{T_M} \frac{\int_0^{T_M} \frac{t'}{\tau} i_M(t') e^{\frac{t'}{\tau}} dt'}{\int_0^{T_M} i_M(t') e^{\frac{t'}{\tau}} dt'} \tag{A.9}$$

depends on the recombination time τ. A linear fit of the (Q, T) experimental points yields a recombination time in the range $\tau = (5 \pm 1)\mu$s. This values was used to determine the initial generated charge $Q(0)$ from Q.

Acknowledgments

This research is partially funded by the European Union (HadronPhysics3 Project No. 283286), the GSI (Darmstadt), within the frame of the Detector technology and systems platform of the Helmoltz association, and the National Institute of Nuclear Physics (INFN), Italy, in the frame of the experiment 3D-SOD. We would like to thank M. Kis, M. Träger and R. Visinka of GSI Detector Laboratory for taking care of the metallizaion of our detectors. This work is also based upon work supported by the Air Force Office of Scientific Research, Air Force Material Command, USAF under Award No. FA9550-15-1-0197 (T.A.). T.A. also acknowledges Bulgarian Science Foundation contract DFNI-E02/6. B.O. acknowledges financial support from Action MP 1208. The authors have also received funding from LASERLAB-EUROPE (proposal LENS002115).

[1] S. Lagomarsino, M. Bellini, C. Corsi, F. Gorelli, G. Parrini, M. Santoro, and S. Sciortino, Three-dimensional diamond detectors: Charge collection efficiency of graphitic electrodes, Appl. Phys. Lett. 103 (2013) 233507 ; doi: 10.1063/1.4839555.

[2] G. Conte, P. Allegrini, M. Pacilli, S. Salvatori, T. Kononenko, A. Bolshakov , V. Ralchenko, V. Konov, Three-dimensional graphite electrodes in CVD single crystal diamond detectors: Charge collection dependence on impinging beta-particles geometry, Nucl. Instr. Meth A 799 (2015) 10-16;doi:10.1016/j.nima.2015.07.024.

[3] F. Bachmair, L. Bä ni, P. Bergonzo, B. Caylar, G. Forcolin, I. Haughton, D. Hits, H. Kagan, R. Kass, L. Lie, A. Oh, S. Phan, M. Pomorski, D.S. Smith, V. Tyzhnevyi, R. Wallny, D. Whitehead, A 3D Diamond Detector for Particle Tracking, Nucl. Instr. Meth. A786 (2015) 97-104; doi: 10.1016/j.nima.2015.03.033

[4] S. Lagomarsino, M. Bellini, C. Corsi, S. Fanetti, F. Gorelli, I. Liontos, G. Parrini, M. Santoro, S. Sciortino, Electrical and Raman-imaging characterization of laser-made electrodes for 3D diamond detectors, Diamond Relat. Mater. 43 (2014) 23-28.

[5] M. Shimizu, Y. Shimotsuma, M. Sakakura, T. Yuasa, H. Homma, Y. Minowa, K. Tanaka, K. Miura, and K. Hirao, Opt. Exp. 17 (2009) 46.

[6] T. V. Kononenko, P. N. Dyachenko, V. I. Konov, Optics Letters 39 (2014) 6962-6965; doi: 10.1364/OL.39.006962.

[7] V. I. Konov, Laser Photonics Rev. 6 (2012) 739 .

[8] Stefano Lagomarsino, Marco Bellini, Chiara Corsi, Vladimir Cindro, Keida Kanxheri, Arianna Morozzi, Daniele Passeri, Leonello Servoli, Christian J. Schmidt and Silvio Sciortino, Radiation hardness of three-dimensional polycrystalline diamond detectors , Appl. Phys. Lett.106 (2015) 193509; doi: 10.1063/1.4921116.

[9] Jan Isberg, Johan Hammersberg, Erik Johansson, Tobias Wikström, Daniel J. Twitchen, Andrew J. Whitehead, Steven E. Coe, Geoffrey A. Scarsbrook, High Carrier Mobility in Single-Crystal Plasma-Deposited Diamond, Science 297 (2002) 1670-1672, doi: 10.1126/science.1074374,

[10] Bangshan Sun, Patrick S. Salter, and Martin J. Booth High conductivity micro-wires in diamond following arbitrary paths, Appl. Phys. Lett., 105 (2014) 231105.

[11] H. O. Jeschke, M. E. Garcia, and K. H. Bennemann, Microscopic analysis of the laser-induced femtosecond graphitization of diamond, Phys. Rev. B 60, R3701(R) (1999).

[12] H.O. Jeschke, M.E. Garcia, K.H. Bennemann, Theory for laser-induced ultrafast phase transitions in carbon, Appl. Phys. A 69 [Suppl.], S49-S53 (1999).

[13] D. M. Rayner, A. Naumov and P. B. Corkum, Ultrashort pulse non-linear optical absorption in transparent media,Opt. Exp. 13 (2005) 3208-3217. 3208.

[14] J. Fink, H. Kruger, P. Lodomez, N. Wermes, Nucl. Instr. Meth. A 560 (2006) 435-443.

[15] T. Apostolova and Y. Hahn, J. Appl. Phys. **88**, 1024 (2000).

[16] A. Kaiser, B. Rethfeld, M. Vicanek and G. Simon, Phys. Rev. B **61**, 11437 (2000).

[17] M. Lenzner, J. Krüger, S. Sartania, Z. Cheng, Ch. Spielmann, G. Mourou, W. Kautek, and F. Krausz, Phys. Rev. Lett. **80**, 4076 (1998).

[18] P. P. Rajeev, M. Gertsvolf, P. B. Corkum, and D. M. Rayner, Phys. Rev. Lett. **102**, 083001 (2009).

[19] M. Hohenleutner, F. Langer, O. Schubert, M. Knorr, U. Huttner, S. W. Koch, M. Kira and R. Huber, Nature **523**, 572 (2015).

[20] W. Slaslow, T. K. Bergstresser and M. Cohen, Phys. Rev. Lett. **16**, 354 (1966).

[21] G. Pennington and N. Goldsman, Phys. Rev. B **64**, 045104(2001)

[22] J. B. Krieger and G. J. Iafrate, Phys. Rev. B **33**, 5494 (1986).

[23] L. V. Keldysh, Sov. Phys.-JETP **20**, 1307 (1965).

[24] G. Wachter, C. Lemell, J. Burgdörfer, S. A. Sato, X.-M. Tong, and K. Yabana, Phys. Rev. Lett. **113**, 087401 (2014).

[25] I. Franco, M. Shapiro, and P. Brumer, Phys. Rev. Lett. **99**, 126802

[26] C. Mézel, G. Duchateau,G. Geneste and

[27] V. E. Gruzdev, Phys. Rev. B **75**, 205106 (2007).

[28] P. G. Hawkins and M. Yu. Ivanov, Phys. Rev. A **87**, 063842

[29] T. Otobe, M. Yamagiwa,J.-I. Iwata, K. Yabana, T. Nakatsukasa,

[30] A. Schiffrin, T. P.-Colberg, N. Karpowicz, V. Apalkov, D. Gerster, Nature **493**, 70 (2013).

[31] R. A. Smith. Semiconductors. 2nd ed. (Cambridge University,

[32] L. S. Pan, D. R. Kania. Diamond: electronics properties and

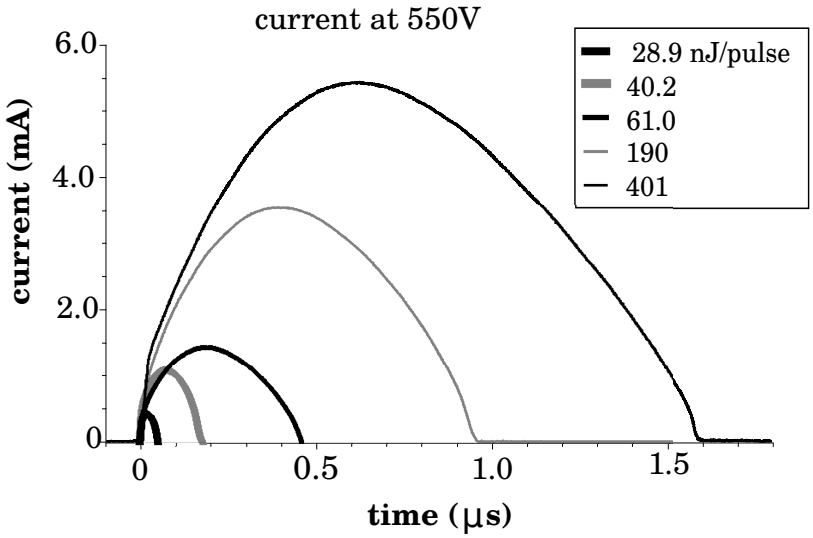

FIG. 1: Current waveforms at 550 V at various intensities at focus.

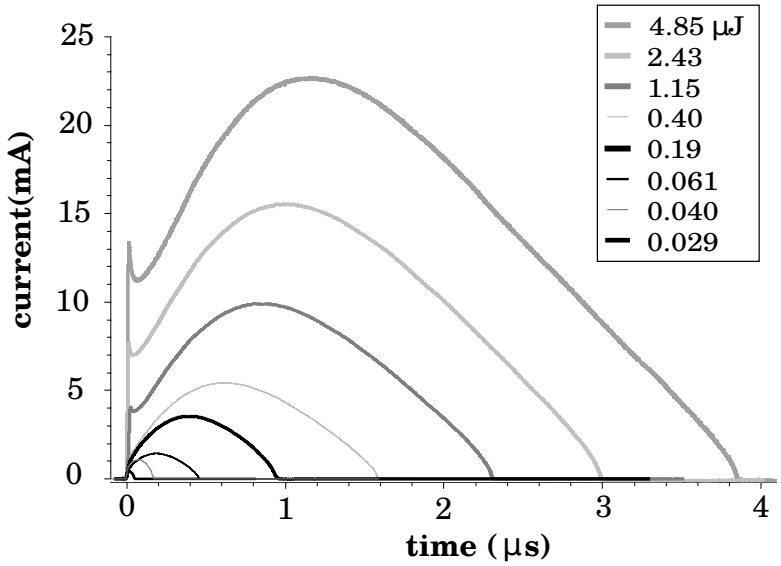

FIG. 2: Current waveforms at 550 V at the highest intensities.

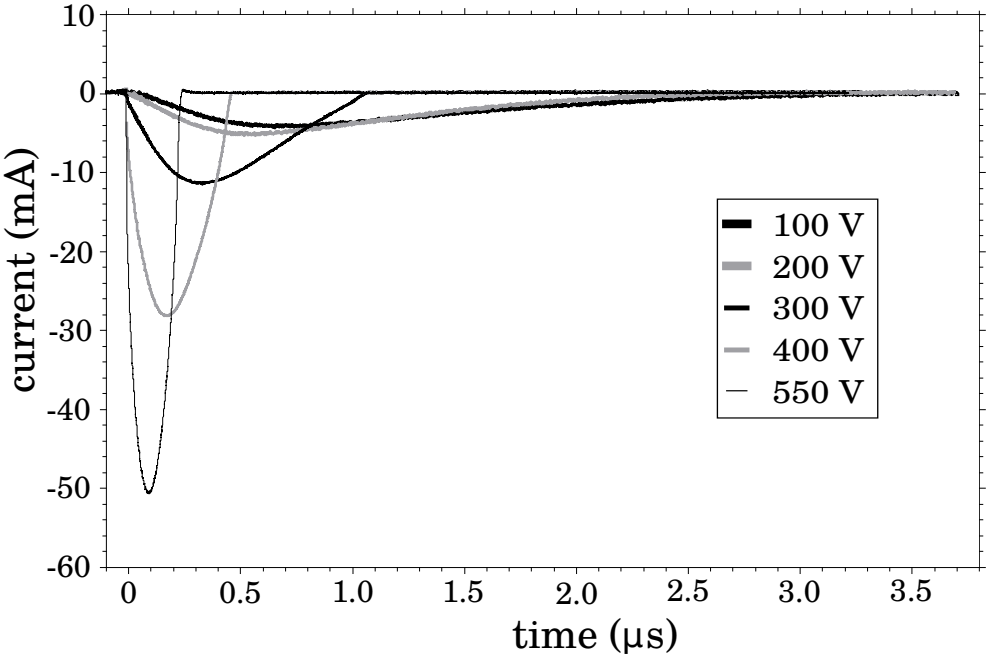

FIG. 3: Current waveforms at different voltages at E=8 nJ.

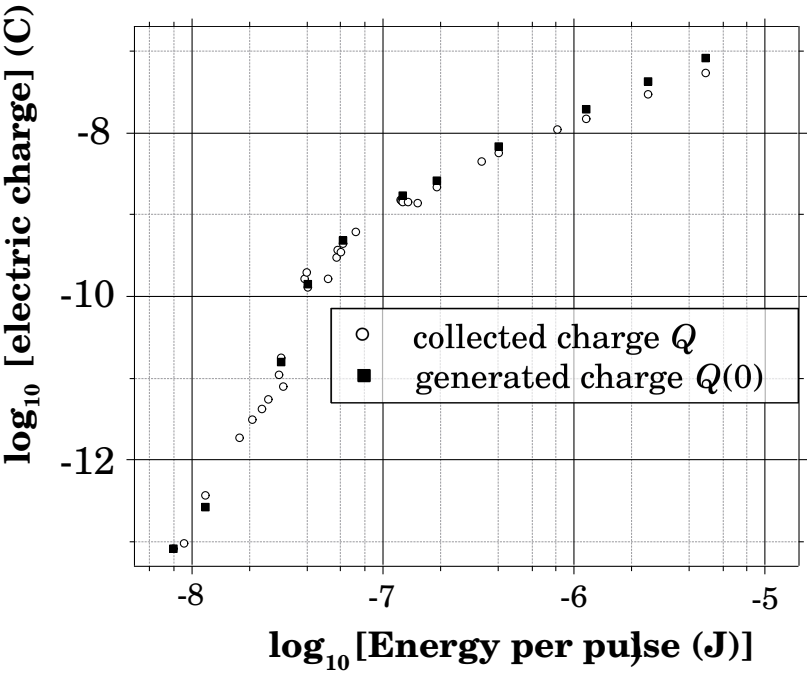

FIG. 4: Current waveforms at 550 V at the highest intensities.

FIG. 5: Modified region after an irradiation of 1.6 μJ/ pulse in a polycrystalline diamond sample. The graphitization has been carried out in order to evaluate the volume of the plasma induced by the laser field in diamond. It has been considered equal to the volume of the graphitized region of a polycrystalline sample obtained using the minimum energy per pulse. Assuming a gaussian beam we obtain $w_0 = 2.5\,\mu$m and $z_R = 35\,\mu$m. These values have been used to determine the carrier density from the measured charge and compare the experimental data to the theory.

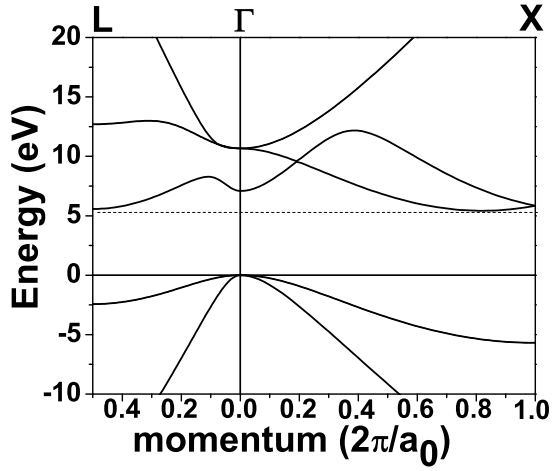

FIG. 6: Static band structure of diamond along the ΓX and ΓL directions in the Brillouin zone. The crystal momentum is given in of units of $2\pi/a_0$.

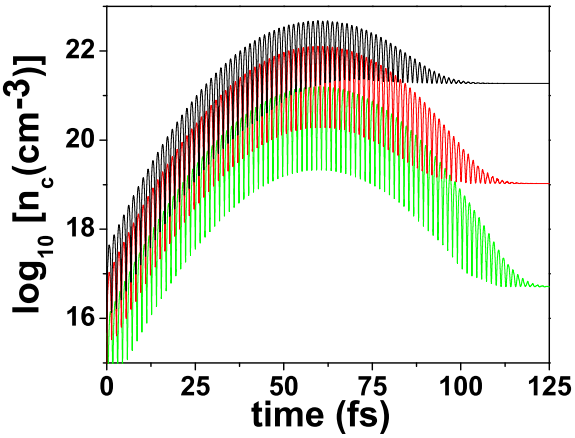

FIG. 7: Time-evolution of the electron density for three different peak intensities of 30fs laser pulse interacting with diamond. $I = 1.5$ TW/cm^2 (dotted line), $I = 10$ TW/cm^2 (dashed line) and $I = 50$ TW/cm^2 (solid line).

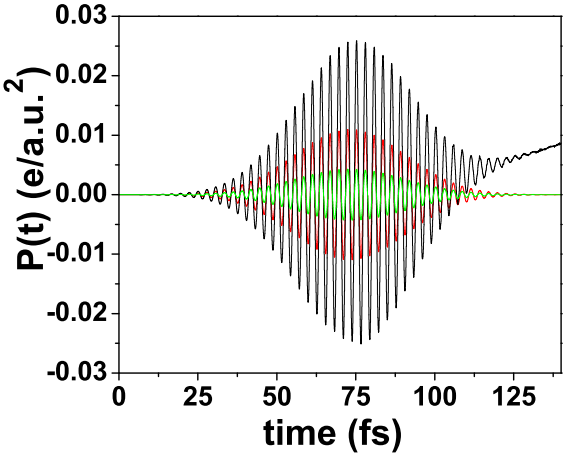

FIG. 8: Time-evolution of the macroscopic polarization density along the laser polarization direction for three different peak intensities of 30fs laser pulse interacting with diamond. $I = 1.5$ TW/cm^2 (green line), $I = 10$ TW/cm^2 (red line) and $I = 50$ TW/cm^2 (black line).

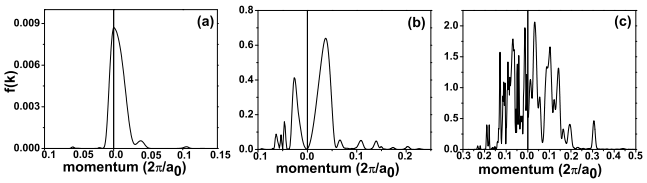

FIG. 9: Momentum distribution of photoionized electrons emerging along the ΓX and ΓL directions after the irradiation of diamond with 30fs laser pulse linearly polarized parallel to bonds between carbon atoms. In Fig.(a), the pulse intensity is $I = 1.5$ TW/cm^2. Fig.(b) and (c) give the same distributions for $I = 100$ TW/cm^2 and $I = 50$ TW/cm^2, respectively. The crystal momentum $\mathbf{k}$ is given in units of $2\pi/a_0$.

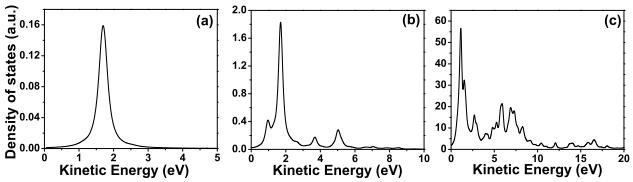

FIG. 10: Density of conduction band states after the irradiation of diamond with 30fs laser pulse linearly polarized parallel to bonds between carbon atoms. In Fig.(a) the peak intensity of the light pulse is $I = 1.5$ TW/cm^2. In Fig.(b) and (c) the peak intensity is $I = 10$ TW/cm^2 and $I = 50$ TW/cm^2, respectively. The kinetic energy of the released electrons is measured relative to the conduction band minimum.

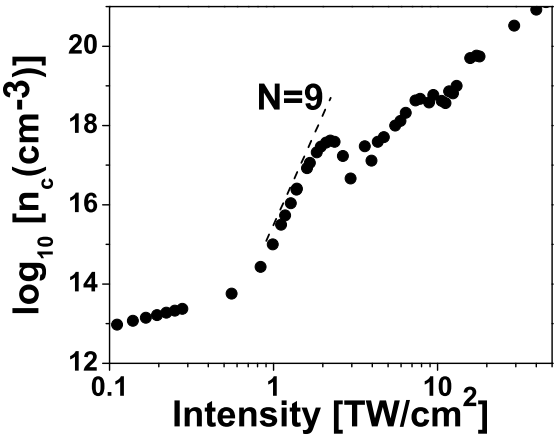

FIG. 11: Intensity dependence of the photoionization yield after the irradiation of diamond with 30fs laser pulse linearly polarized parallel to bonds between carbon atoms.

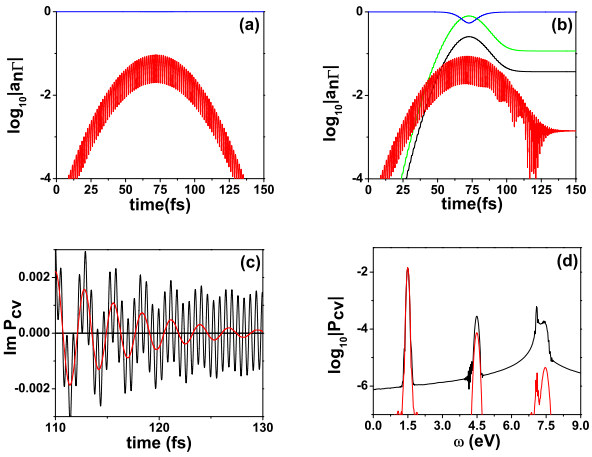

FIG. 12: Perturbative vs. non-perturbative multiphoton ionization of diamond interacting with 30fs laser pulse with intensity = 1.5 TW/cm^2. Fig. (a) Time evolution of the modulus of the Fourier amplitudes $|a_{n\mathbf{k}}|$ in the expansion of the photoelectron wave-packet over Bloch states with $\mathbf{k} = (0, 0, 0)$ by neglecting laser-induced interactions among valence bands (cf. also text). Valence and conduction band amplitudes are given by blue and red lines, respectively. Fig.(b) shows the time evolution of the modulus of the Fourier amplitudes by including laser-induced dipole-dipole interactions between the three valence bands at the Brillouin zone centre (blue,green and black lines), the photoionization amplitude is given by the red line. Fig.(c) shows the imaginary part of the interband polarization by neglecting (red curve) and by including indirect photoionization pathways (black curve) and Fig.(d) gives the frequency-dependence of the modulus of the Fourier transform of the interband polarization.

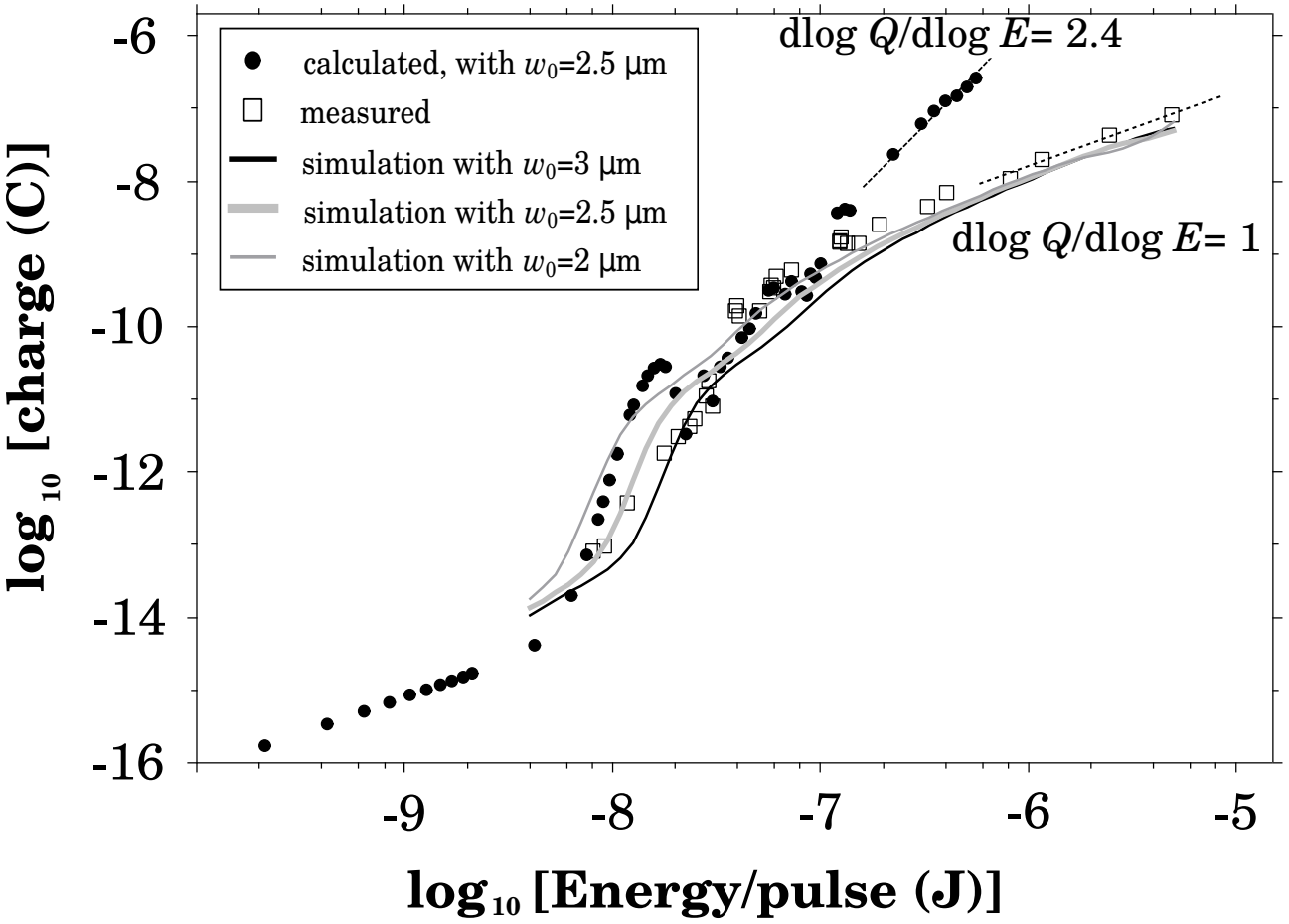

FIG. 13: Comparison of theory and data. Square markers: generated charge as a function of the pulse energy from experimental data. Circles: generated charge derived from the theoretical electron yield in Fig. 11 distributed in an effective ellipsoidal volume of axis $w_0 = 2.5\,\mu$m and $z_R = 35\,\mu$m. Black, gray and light gray lines: charge calculated from Eq. 15 as a function of the pulse energy calculated with Eq. 15 for w_0=2, 2.5 and 3 μm.